Surface & Coatings Technology 467 (2023) 129662

Contents lists available at ScienceDirect

Surface & Coatings Technology

journal homepage: www.elsevier.com/locate/surfcoat

Pretreatment strategies of titanium substrates to modulate the electrochemical properties of CVD-grown Ti-doped diamond electrodes for dopamine detection

Rocco Carcione [a,b,*], Silvia Battistoni [b], Elena Palmieri [a], Silvia Orlanducci [a], Emanuela Tamburri [a,**]

[a] Dip.to di Scienze e Tecnologie Chimiche & UdR INSTM di Roma - Università degli Studi di Roma "Tor Vergata", Via della Ricerca Scientifica, Rome 00133, Italy
[b] Consiglio Nazionale delle Ricerche - Institute of Materials for Electronics and Magnetism (CNR-IMEM), Parco Area delle Scienze 37A, Parma 43124, Italy

ARTICLE INFO

Keywords:
Surface processing
Ti-doping
Conductive diamond films
Dopamine detection

ABSTRACT

The identification of highly sensitive materials able to combine performance stability, relatively low cost, controllable and large area fabrication process is still a major bottleneck in the scientific community. Dopamine is considered a key indicator to monitor cardio and cerebrovascular diseases and its redox activeness makes electrochemical detection the most straightforward and promising sensing approach. Here we report the realization, by a simple yet effective approach, of diamond-based electrodes with a native selectivity towards dopamine. In details, three different substrate pretreatments, i.e., lapping, electropolishing and chemical etching, are adopted to tailor the morphological, structural, and sensing features of titanium doped diamond layers. SEM, AFM, Raman spectroscopy, XRD, XPS and *I-V* analyses demonstrate the features' modulation of the diamond layers being crucial for electrochemical and sensing performances, as confirmed by dopamine selectivity under ascorbic and uric acid interferents' excess. Furthermore, the controlled introduction of oxygen-containing groups enhances the dopamine sensitivity, lowering the detection limit from 6000 to 600 nM. In addition to giving an important insight on the physical-chemical growth processes, these preliminary results pave the way for the exploitation of these materials in a wide range of sensing applications, thanks to the non-toxicity and high surface tunability without post-synthesis treatments.

1. Introduction

In the last years, the search of new materials characterized by high sensitivity and stability for developing electrochemical sensors of biomolecules and neurotransmitters attracted a great attention from the scientific community [1–3]. The increased life expectancy of the population has in fact led to a transition from a situation in which infectious and deficiencies diseases were prevalent to a preponderance of chronic degenerative ones. It is well-known that, in richer countries, the greatest global burden of disease is mainly attributable to cardio, cerebrovascular diseases and neuropsychiatric disorders. In this view, significant efforts are being made to produce devices for monitoring the monoamine dopamine (DA) neurotransmitter, the level of which in biological samples serves as a key indicator to monitor Parkinson's, Alzheimer's and Huntington's diseases, neural crest tumors, multiple sclerosis and stroke, as well as probable drug effects [4–6]. Due to DA inherent redox activeness [5], electrochemistry proved to be the most straightforward and promising approach among the developed methods. However, ascorbic acid (AA) and uric acid (UA) have redox potentials close to that of DA and are characterized by a concentration in biological environments over 100 times higher. Therefore, these analytes behave as typical interferents hindering the DA electrochemical determination [5].

Among the sensing materials for DA detection, boron-doped diamond (BDD) produced by energy-assisted (plasma or hot filament, HF) Chemical Vapor Deposition (CVD) processes is a good candidate for the unique properties such as low background current and adsorption, inherent robustness, wide potential window and good biocompatibility [1–5,7–22]. However, a pure BDD system difficulty distinguishes the

* Corresponding author at: Consiglio Nazionale delle Ricerche - Institute of Materials for Electronics and Magnetism (CNR-IMEM), Parco Area delle Scienze 37A, Parma 43124, Italy.
** Corresponding author.
E-mail addresses: rocco.carcione@imem.cnr.it (R. Carcione), emanuela.tamburri@uniroma2.it (E. Tamburri).

https://doi.org/10.1016/j.surfcoat.2023.129662
Received 6 February 2023; Received in revised form 22 May 2023; Accepted 23 May 2023
Available online 30 May 2023

redox potentials between DA and other interferents [23,24]. Therefore, recent studies have been dedicated to exploring further post-synthesis treatments for BDD surface modifications including anodization [25], hydrogen plasma [26], etching into porous forms [9], carbon-based nanomaterials [5,8], polymer films [27] and nanoparticles [5,8,28,34]. However, it is worthy to recall a series of controversies related to the use of boron to achieve diamond doping. First, a strong B doping level generally compromises the quality and conduction behavior of diamond lattice as it induces more scattering and a subsequent lowering of charge carriers mobility [29,30]. Grain boundaries, intra-grain dislocations, intergranular amorphous carbon or graphitic regions and hydrogen trapping are in fact the common defects produced by a 10^{20} cm^{-3} doping level [13,31]. Under these conditions, the electrochemical mechanism of heterogeneous electron transfer to a diamond surface turns out to be largely dominated by a conduction via impurity band or surface states [32,33]. Additionally, considering that the handling of boron compounds represents a serious risk for the health, it is evident that the use of BDD for developing electrochemical sensors can become quite hazardous [34].

To overcome these criticalities, an interesting new strategy is to produce conductive boron-free diamond by a proper insertion of foreign doping species within the diamond lattice directly during a CVD synthesis processes [35,36]. In this context, many efforts have been dedicated to produce conductive diamond films containing Nd, N, Ti and hybrid Si-Ni entities on a variety of substrates such as silicon, titanium, niobium, tantalum, molybdenum, glassy carbon [36–41]. In particular, the doping with Ti species was interesting for the intrinsic biocompatibility of this element [42–45]. Moreover, it was demonstrated that Ti-doped diamond layers grown on Ti substrates allow for assembling electrodes competitive in terms of electrochemical performances with respect to commercial BDD ones [35,36] and as fundament of electronic devices [46]. Another very important aspect to consider is that CVD methods are powerful approaches to tailor a complex range of diamond properties such as dopant concentration, crystallographic defects, sp^2 and amorphous carbon content, amount of grain boundaries and surface terminations (H, O) [22,47,48]. The synergistic contribution of overall these factors is crucial to define the electronic and electrochemical properties of the diamond phase [49,50]. In particular, the tailoring of the surface terminations is functional to control the selectivity of diamond electrodes, due to the electrochemical reactions that take place at the interface between electrode and electrolyte solution [13]. In fact, it is well established that H-terminations lead to non-polar, hydrophobic diamond surfaces with high conductivity and low charge transfer resistance [16,51]. Conversely, the presence of O-terminations hinders the electron transfer rate of certain redox couples, providing enhanced electroanalytical selectivity for specific electrochemical analytes [25,52]. In this scenario, different strategies have been settled to customize the diamond surface according to the specific application. For H-sites increase, electrochemical methods (water reduction) or radio frequency H-plasma treatments are typically adopted [13,53]. Chemical routes by boiling in oxidizing acids, photochemical or thermal oxidation, oxygen plasma or UV-ozone treatments and anodic electrochemical polarization are the principal methods used to oxidize diamond samples [54–67]. However, some limitations relate to these conventional procedures. For example, Xu et al. [68] demonstrated that hydrogen plasma treatments favor the formation of hydrogenated amorphous layers that can be easily exfoliated from the diamond surface. Similarly, oxidative processing can produce graphitization and etching of the diamond phase, thus modifying the surface roughness and quality of the diamond films [55,69–71], or can induce a degree of oxidation so high to strongly decrease the electrochemical activity of the diamond layers [57,72].

To the best of our knowledge, boron-free diamond electrodes have never been used for DA detection. Therefore, the approach here proposed is to explore how titanium substrates pretreatments can tailor the morphological, structural, and functional features of Ti-doped CVD-diamond as sensing platform for DA electrochemical detection under AA and UA excess and with a limit of detection (LOD) comparable with that of unmodified BDD [4,5,7–9,73]. Namely, a combination of physical and chemical procedures, including lapping, electropolishing and chemical etching, was investigated to proper modulate the surface of Ti substrates. SEM, AFM, Raman spectroscopy, XRD and XPS techniques were utilized to thoroughly study the properties of the produced diamond coatings, which have been correlated to the surface modifications of the Ti substrates. I-V measurements and electrochemical tests were performed to characterize the diamond layers as conductive materials. Finally, the performance as electroanalytic sensors' electrode was definitively assessed by estimating the selectivity for the DA determination under the presence of the interfering AA and UA compounds. The collected results clearly indicate the possibility to use Ti-doped diamond as sensing material for those applications where high biocompatibility and nontoxicity are required.

2. Experimental

2.1. Chemicals

$HClO_4$, methanol, n-butanol, potassium ferrocyanide, potassium chloride, uric acid (UA), L-(+)-ascorbic acid (AA), dopamine hydrocloride (DA), sodium hydroxide (NaOH) and phosphate buffered saline (PBS) pellets were purchased by Merck KGaA and used as received. All the solutions are prepared in distilled water.

2.2. Pre-deposition treatments of Ti substrates

Titanium substrates were produced by cutting a 0.5 mm thick polycrystalline titanium foil in 1.5 cm × 1.5 cm squares that were flatted by a hydraulic press at a pressure of few MPa. The substrates were subjected to subsequent surface modification treatments to modulate their reactivity towards the diamond deposition. These treatments were carried out using physical and chemical approaches that include: i) a lapping procedure at a 35 rpm speed and a 11 MPa pressure by using an abrasive SiC foil; ii) an electropolishing process by applying a 20 V potential for 15 min at −30 °C in a solution of 12 M $HClO_4$ ($6\%_{v/v}$), methanol ($59\%_{v/v}$) and n-butanol ($35\%_{v/v}$) [73]; iii) an electropolishing followed by immersion in a 2 M NaOH solution for 1 h at 80 °C.

2.3. Diamond growth

The Ti-doped diamond samples were synthetized by using a customized hot filament CVD apparatus, furnished of a powder-flowing chamber properly designed to insert foreign species within the diamond lattice directly during the synthetic process by gas phase. The experimental conditions for deposition were previously optimized and can be found elsewhere [35]. Briefly, here we can recall that to achieve the Ti doping, N_2 gas fluxes are employed to carry Ti(*IV*) acetylacetonate powders from a reservoir to the deposition chamber. A nozzle below the hot filament allows for spreading the carrier flow across the active area of the heated Ti substrate, where diamond is being deposited. This configuration enables thermal decomposition of the metal-containing precursors and a uniform distribution of the metallic species within the growing diamond lattice. The produced samples were named D_LAP, D_EP, and D_NaOH depending on whether the Ti substrates were subjected to lapping, electropolishing, or electropolishing followed by immersion in NaOH solution, respectively. The reproducibility of the whole process was checked by producing three replicas for each type of sample.

2.4. Characterization techniques

A Hitachi S-4000 Field Emission Scanning Electron Miscroscope (FE-SEM) was employed to acquire the Scanning Electronic Microscopy (SEM) images. A Solver Px Scanning Probe Microscope from NT-MDT

was used to record the Atomic Force Microscopy (AFM) images. The AFM measurements are performed in semi-contact mode by means of a silicon tip (NSG10, force constant ~12 N/m, resonant frequency 220 KHz) having a nominal radius of less than 10 nm. Each sample was analyzed in different areas by scanning 20 μm × 20 μm zones. A Horiba Xplora One™ Raman Microscope was used to collect Raman spectra under a 532 nm laser source, by setting the on 2400 grooves/mm. Each single peak was deconvolved with a Lorentzian line shape that allows to derive position, intensity, and full width at half maximum (FWHM) parameters for each signal in the spectra. A Seeman–Bohlin X-ray diffractometer (grazing angle configuration) was exploited for X-ray diffraction (XRD) measurements. Cu Ka (λ = 1.5406 Å) radiation was employed in steps of 0.02° operated at 40 kV and 30 mA. A KRATOS Axis Ultra DLD apparatus was used for the XPS measurements by using X-ray beam from Al target (15 kV, 10 mA). The electron energy analyzer worked by setting the pass energy at 20 eV and the step size at 0.05 eV. Casa-XPS software deconvolved the core level C1s spectra with line shapes having both Gaussian and Lorentzian character, after performing a Shirley background subtraction in the spectral interval between 281 and 291 eV. *I-V* measurements were performed by means of a four-points apparatus, providing CVD-diamond surfaces with four metallic contacts (Au-coated Cu microtips), by measuring the current signal driven by a DC voltage generator. To evaluate the electrochemical performances of CVD-diamond, cyclic voltammetry (CV) and square wave voltammetry (SWV) measurements were carried out in a standard one-compartment three-electrode cell by using a Palm Sense compact electrochemical workstation. A saturated calomel electrode (SCE) and a Pt foil were used as the reference and counter electrodes, respectively. To realize the working electrodes, the Ti-doped diamond samples were provided with a platinum electric contact on the back side of the Ti substrates. To rule out the possible contribution of the titanium substrates to the Ti-doped diamond electrochemical response, all the metal portions of the assembled electrodes were coated by an epoxy layer. The amplitude (A), frequency (f), and step potential (ΔEs) of the staircase waveform experimental parameters were optimized as follows: $A = 30$ mV, $f = 5$ Hz, $\Delta Es = 2$ mV for D_EP and D_NaOH films, by using a 10 μM DA in 10 mM PBS solution at pH 7.4. Electrochemical impedance spectroscopy (EIS) measurements were performed between the frequency range of 1.0 and 50,000 Hz in PBS 10 mM solution by applying a sinusoidal wave of 50 mV of amplitude superimposed to a 0 V bias and the resulting curves were analyzed using the PSTrace software. In all electrochemical and impedimetric tests, the area of the diamond electrodes exposed to the electrolyte was 1 cm^2. The overall measurements were conducted at R.T.

3. Results & discussion

In Fig. 1 are shown the SEM and AFM images of the Ti substrates treated by lapping (Ti-LAP), electropolishing (Ti-EP), and electropolishing followed by immersion in NaOH solution (Ti-NaOH) along with the corresponding diamond coatings.

From Fig. 1a we can distinguish the modifications of Ti substrates induced by pretreatments. While the surface of Ti-LAP is characterized by a uniform distribution of micro-sized grooves, a very smooth finishing is shown by Ti-EP because of the electropolishing processing able to produce mirror-like surfaces [74]. As expected, the NaOH chemical etching models the electropolished flat surface, producing a micro-sculpturing for Ti-NaOH. Regardless of the surface morphology, continuous and uniform polycrystalline layers are found to grow on all Ti substrates (Fig. 1b), even if specific textures are evident for every sample. As highlighted in the inserts in Fig. 1b, the D_LAP and D_EP films are formed by grains with well-facetted triangular features ranging from 0.5 to 1.0 μm. Conversely, the D_NaOH sample's morphology shows a consistent secondary nucleation crystals growth which reduces the average grain size to the nanoscale. These results are consistent with those of the AFM investigation which confirms that D_LAP and D_EP are formed by a compact assemble of submicrometric conical structures, while D_NaOH shows nanometric diamond grains with a less defined shape (Fig. 1c). By averaging over several AFM images, values of surface root mean square roughness (Sq), average height (Sa) and height difference between the highest and lowest points on the surface (St) were determined and reported in Fig. 1d. These data allow for a quantitative comparison of the different samples and clearly indicate that D_EP is that for which the diamond coating, similarly to its substrate, exhibits the smoothest surface with Sq, Sa and St values of around 180, 170 and 700 nm, respectively. While the Sq and Sa values of D_LAP and D_NaOH are only slightly greater than that of D_EP (220 and 230, 250 and 240 respectively), the peak-to-valley distance St is found to be 1.2 μm for D_LAP and 1.4 μm for D_NaOH. The high roughness of these samples can be reasonably explained by the ability of CVD diamond to reproduce the surface characteristics of the substrate on which it is grown.

The crystalline quality of the diamond coatings was assessed by Raman spectroscopy and X-ray diffraction (Fig. 2). For each sample five Raman spectra from different microregions were collected and analyzed. Representative normalized and deconvolved Raman spectra of D_LAP, D_EP, and D_NaOH are reported in Fig. 2a.

Each spectrum was deconvolved by five Lorentzian lines corresponding to the diamond line at 1332 cm^{-1}, the D and G bands at about 1350 and 1570 cm^{-1} respectively, and the ν_1 and ν_3 bands at about 1150 and 1490 cm^{-1} assigned to transpolyacetylene segments vibrations [74–78]. Due to the doping process and the mismatch between thermal expansion coefficients of diamond and titanium [35,79,80], the signal ascribable to the diamond line is found at 1333.1, 1336 and 1341 cm^{-1} for D_LAP, D_EP and D_NaOH, respectively. For each sample the diamond volume fraction (Σ_d) was calculated following the procedure described in Refs [81, 82]. Σ_d values of 90, 93 and 81 % were collected for D_LAP, D_EP and D_NaOH, respectively. The remarkable percentage of D_EP denotes that this sample is given by a diamond phase without significant contents of graphite and/or amorphous carbon. Analogously, a value of about 11 cm^{-1} for the FWHM of the diamond line indicates a good CVD-diamond quality for this sample. Conversely, the lower percentage (i.e., 81 %) and higher FWHM value (ca. 19 cm^{-1}) found for D_NaOH can be explained by the formation of a sp^2 carbon phase at the boundaries of the nanometric diamond grains of this sample.

Further structural information can be achieved by the XRD analysis. XRD patterns of D_LAP, D_EP and D_NaOH along with the diffraction signals' assignment are shown in Fig. 2b. All the samples show the intense diffraction peaks ascribed to the TiC interlayer produced on Ti substrates at the beginning of the deposition process. The (111) and (220) diamond reflections are located at 2ϑ diffraction angles of 43.9° and 75.3°, which are slightly higher than those typical of a pure diamond phase [35]. This effect was previously explained on the basis of the diamond lattice constant's enlargement, reasonably due to the incorporation of Ti dopant entities [35]. The Scherrer equation provides the crystallite mean size from the position (2ϑ) and FWHM of the (111) reflection (for details see Supporting Information) with values of 35.2, 41.7 and 21.8 nm for D_LAP, D_EP, and D_NaOH, respectively. This result confirms once again that the diamond deposit with the higher crystallinity grows on the electropolished titanium substrate, and the active role played by the solid substrate in the heterogeneous deposition from the gas phase. This outcome is not at all unexpected, considering that the heterogeneous nucleation of diamond is critically influenced not only by the density of the substrate surface defects acting as nucleation sites, but also by the surface nucleation rate [83,84]. Finally, it is worthy to note that no signals related to crystalline graphite and/or Ti phases are found in the spectra confirming the good phase purity of all the diamond deposits.

An in-depth investigation on the elemental composition and chemical state of diamond surfaces was performed through a XPS study (Fig. 3).

The survey spectra of the D_LAP, D_EP and D_NaOH samples (Fig. 3a) were analyzed by referencing the peak related to the C 1s level of diamond at 285 eV [85,86]. On this basis, the signal located at around 532

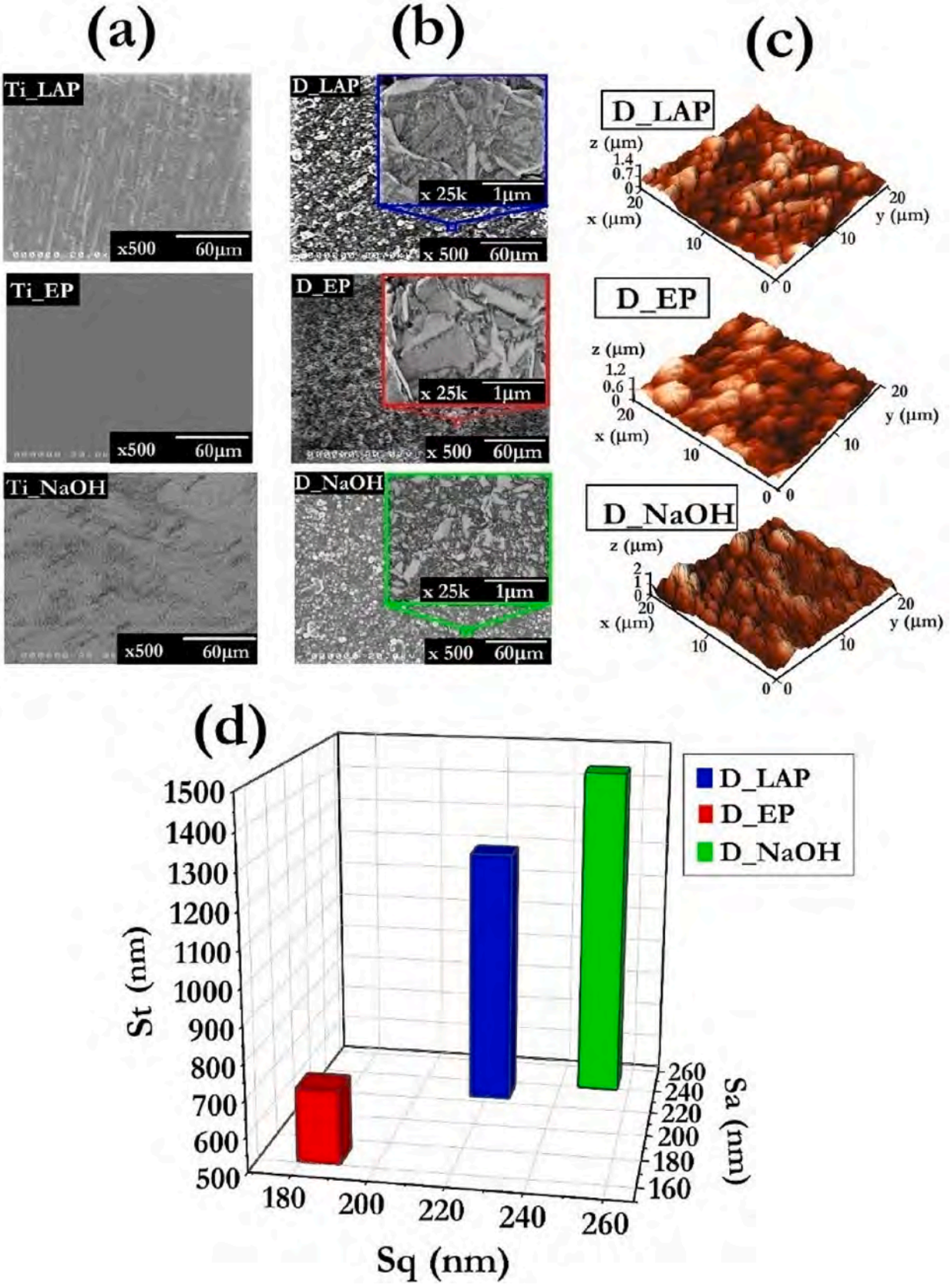

Fig. 1. SEM images acquired for (a) Ti substrates treated by lapping (Ti-LAP), electropolishing (Ti-EP), and electropolishing followed by immersion in NaOH solution (Ti-NaOH); (b) respective diamond coatings (D_LAP, D_EP, and D_NaOH samples). Insets: SEM images of the diamond grains taken at high magnification. (c) Three-dimensional AFM topography images of D_LAP, D_EP and D_NaOH diamond films. The *Z*-axis scales are different for the three images. (d) 3D-graph showing the values of surface root mean square roughness (Sq), average height (Sa) and height difference between the highest and lowest points on the surface (St).

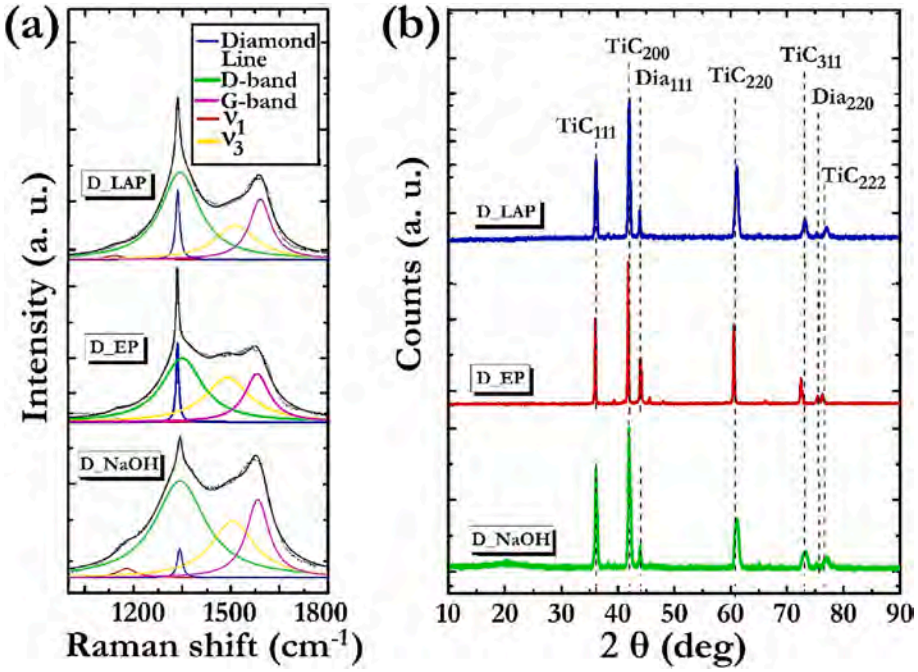

Fig. 2. (a) Representative deconvolved Raman spectra and (b) XRD patterns of D_LAP, D_EP and D_NaOH samples along with signals' attribution.

eV is assigned to the oxygen O 1s, reasonably due to carbon atoms in oxidized configurations. The black dashed square outlines the region between 440 and 460 eV, in which the Ti 2p signals are commonly reported in the literature. As it can be seen, the absence of such signals from the diamond surfaces confirms that the diamond layers form a uniform coating of the Ti substrates and suggests that the Ti species produced by the decomposition of the metalorganic precursor are in some way distributed within the diamond lattice. The quantitative analysis of the experimental data provides a surface elemental composition of about 98 % C and 2 % O for both D_LAP and D_EP. Conversely, 91 % C and about 9 % O are detected for D_NaOH. To better detail the surface chemistry, the high-resolution XPS C 1s spectra were deconvolved and analyzed (Fig. 3b). From the analysis of the peaks at 284.3, 284.8, 285.3 and 286.8 eV, the C═C, C—C, C—H_x and C—O bonds were respectively recognized. A panoramic view of the relative abundance of the main C configurations is illustrated in the histogram graph of Fig. 3c. It is worthy to note that no C═C bonds were detected for D_LAP and D_EP, while a ~4 % amount was found for D_NaOH. As previously discussed, the reduced diamond grains' size with the related increase of grain boundaries can explain the presence of sp^2 or amorphous carbon domains on this latter sample. Basically, all the diamond layers exhibit the same degree of C-H_x terminations, in line with the values found for HFCVD-grown diamond. However, while D_LAP and D_EP deposits are constituted by a rather similar surface composition, with an abundance of around 60, 40 and less than 2 % for the C—C sp^3, C—H_x and C—O configurations respectively, a quite different situation arises for D_NaOH. This sample shows a 40 % abundance for the C—C sp^3 and a ~10 % relative concentration of C—O bonds (for details see Supporting Information). The larger degree of surface oxidation exhibited by D_NaOH can be tentatively rationalized as a consequence of the NaOH pretreatment of Ti substrate that enables the formation of surface titanium oxides. In this view, during diamond deposition the O-containing radical species formed from the interaction between H• and $CH•_3$ radicals with the titanate groups are thus expected to interact with the growing diamond phase by grafting the C• terminations and leading to surface oxygenated functional groups. In Fig. 3d a possible mechanism for diamond growth and functionalization under these experimental conditions is depicted.

Current-voltage (*I-V*) measurements in the (0÷0.8) V potential range were performed to correlate the electrical features with the samples' morphology, topography and surface chemistry. In Fig. 4a, b the electrical conductivity is reported as a function of the parameters derived by the structural, topographical and surface chemistry analyses of the Ti-doped diamond layers.

As a general trend, the conductivity values are found to increase with the diamond phase (Σ_d%) content and the averaged dimension of crystallite domains (τ) (Fig. 4a). In fact, we note that D_LAP and D_EP, which are characterized by higher Σ_d% and τ, show a conductivity in the range $(0.8 \div 1) \times 10^4$ S/cm. A σ of about an order of magnitude lower is exhibited by D_NaOH which shows the larger concentration of amorphous and graphitic carbon phases and the lowest grain size. These results can be explained by assuming that the contribution of C sp^2 to the total charge transport properties can be considered negligible, while the amplification of the grain boundary scattering, due to the relatively small size of the crystallites, plays a fundamental role in increasing the electrical resistivity. On the other hand, one can observe that the surface roughness profile has a no clear impact on the electrical behavior (Fig. 4b). In particular, while the σ values are fairly close for D_LAP and D_EP, the peak-to-valley distance (St) of D_LAP is almost the double than that of D_EP. Conversely, even showing the lowest σ, D_NaOH is characterized by a St value similar to that of D_LAP. A different result is obtained as regards the surface chemistry. In this case, a consistent surfaces oxidation degree is effective in reducing the electrical conductivity, as demonstrated by D_NaOH which exhibits a C—O terminations' abundance four times greater than that of the other two samples.

All the collected results convincingly demonstrate that the developed methodology for growing electroconductive diamond systems also enables to selectively tune their surface oxidation grade without performing a post-synthesis processing, that could influence the structural quality of the produced materials. In particular, the introduction of oxygenated groups can be considered an added value for the exploitation of Ti-doped diamond as a sensing platform, since the presence of singly bonded C—O moieties has been found crucial for the electrochemical activity of diamond materials [57,72]. Considering that D_LAP and D_EP have showed very similar structural, surface chemistry and charge transport properties, in the following it was decided to carry out an in-depth electrochemical study only on D_EP and D_NaOH aimed at evaluating the feasibility of using such boron free conductive diamonds

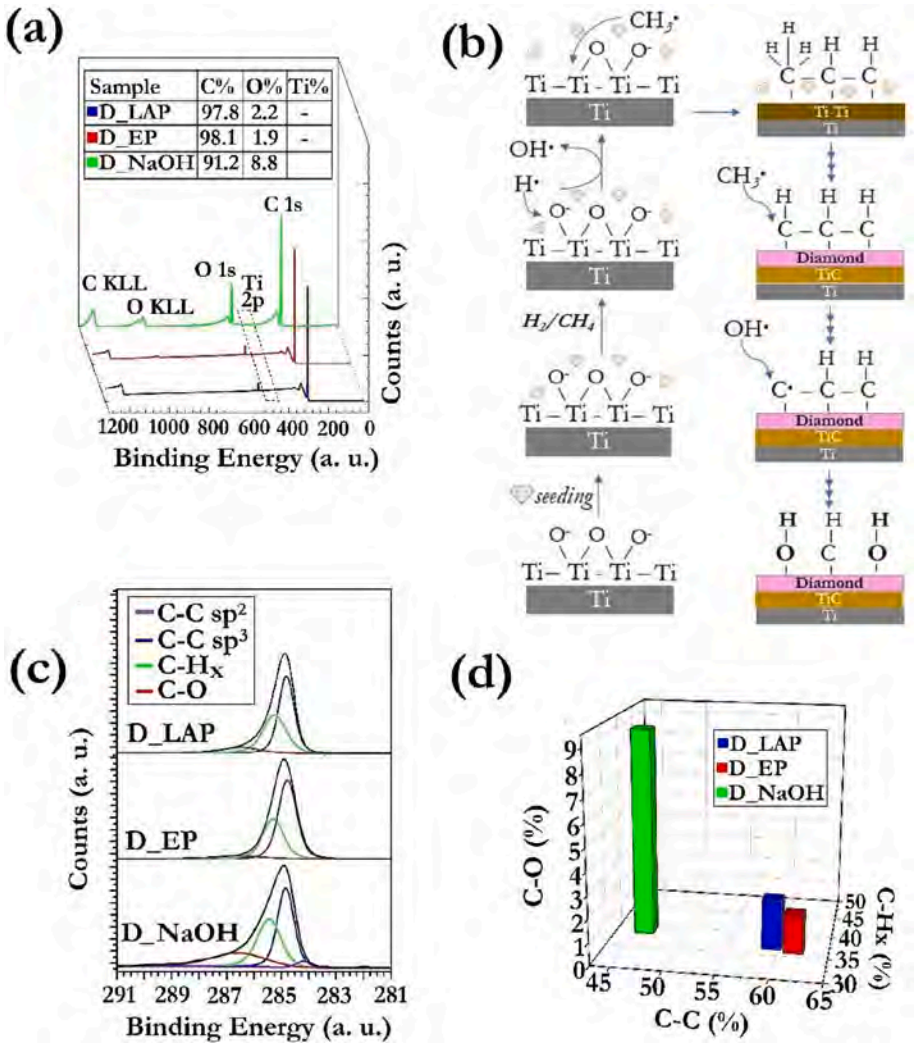

Fig. 3. (a) XPS survey spectra of D_LAP, D_EP and D_NaOH samples along with surface elemental composition in the inset; (b) possible reaction mechanism for the growth of diamond on titanium surfaces modified by the NaOH activation; (c) deconvolved high resolution XPS spectra of C 1s core levels along with signal attribution; (d) 3D-graph displaying the relative abundance of the C arrangements on the D_LAP, D_EP and D_NaOH samples' surfaces.

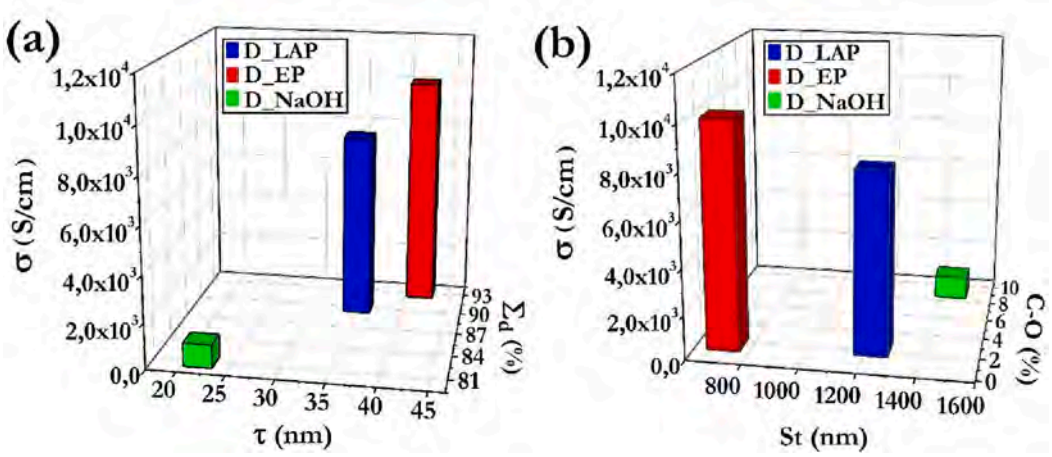

Fig. 4. Histogram graphs showing the trend of the conductivity as a function of (a) the structural features and (b) the topographical and surface chemistry properties of the diamond layers.

as electrodes for dopamine detection.

The electrochemical response was firstly checked in a 10 mM PBS physiological environment. In Fig. 5a, b the CV curves recorded at 5, 10, 15, 30, 60, 120 and 200 mV s^{-1} within the (−0.5 ÷ +1.0) V potential range by D_EP and D_NaOH samples are reported.

We observe that larger capacitive currents are found for D_NaOH,

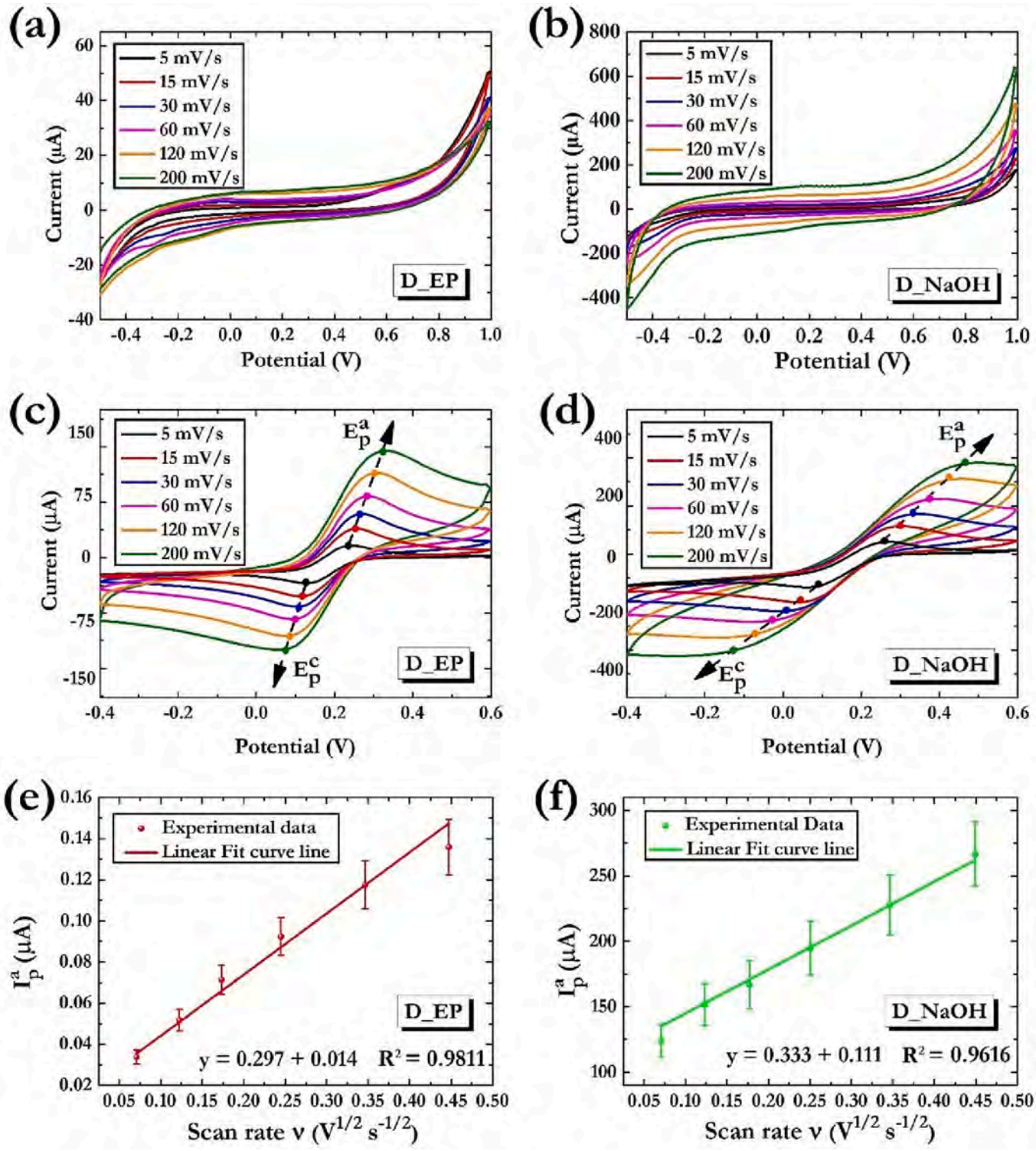

Fig. 5. CV curves collected in the range between −0.5 and +1.0 V in 10 mM PBS at 5, 10, 15, 30, 60, 120 and 200 mV s^{-1} by (a) D_EP and (b) D_NaOH electrode. CV curves for 10 mM $[Fe(CN)_6]^{4-}$ in a 0.1 M KCl solution at various scan rate (5, 15, 30, 60, 120 and 200 mV s^{-1}) in the potential range between −0.4 and +0.6 V collected by (c) D_EP and (d) D_NaOH electrode; anodic peak currents as a function of the scans rates' square root for (e) D_EP and (f) D_NaOH.

probably due to its higher surface roughness even if the occurrence of some space charge regions into the material responsible for a charge carriers' density decreasing cannot be neglected. As shown in Fig. 5a, b, spurious peaks are absent in the CV curves of both the electrodes, pointing out that both D_EP and D_NaOH samples surfaces are devoid of electrochemically active functionalities, that can hinder electroanalytical detection procedures.

To further test the electrodes performance, the electrochemical response of the ferro-ferricyanide $Fe(CN)_6^{3-/4-}$ chemical species, a standard outer sphere redox couple, was investigated [30]. Fig. 5c, d shows the typical CV curves recorded at scan rates ranging from 5, 15, 30, 60, 120 up to 200 mV s^{-1} by a 10 mM $Fe[(CN)_6]^{4-}$ in a 0.1 M KCl solution. The corresponding values of the anodic and cathodic peak potential difference (ΔEp), the ratio between anodic and cathodic peaks'

currents (I_a^p/I_c^p), and the linear variation of I_a^p versus the square root of the scan rates ($\nu^{1/2}$) (Fig. 5e, f) for both D_EP and D_NaOH electrodes are in agreement with a quasi-reversible process. To estimate whether a slow kinetics or a solution uncompensated resistance drives the quasi-reversible reaction, the apparent heterogeneous electron-transfer rate constant, k^0_{app}, was calculated by analyzing the variation of ΔE_p with the scan rate according with the Nicholson method. The elaboration of the acquired data gave k^0_{app} values of 2×10^{-2} and 1×10^{-3} cm s^{-1} for D_EP and D_NaOH, respectively. These different rate constant values indicate that the D_EP electrode exhibits a higher kinetics than the D_NaOH one. This finding concords with other studies in the literature, which demonstrated that the diamond electrodes functionalized with oxygen-containing groups hinder the k^0_{app} of the $Fe[(CN)_6]^{3-/4-}$ redox couple [3,4,87,88].

The ability to detect DA was tested in a 1 mM solution of this neurotransmitter in a 10 mM PBS solution at pH 7.4. The voltammograms recorded at the scan rate of 15, 30, 60, 120 and 200 mV s^{-1} by D_EP and D_NaOH are shown in Fig. 6. The potential range between −0.2 V and +0.8 V was purposefully selected to avoid further dopamine-o-quinone reactions, that can involve the formation of melanin-like polymeric species on the diamond electrode surface, producing its fouling [4].

Analogously to what found for the $Fe(CN)_6^{3-/4-}$ couple, the values of ΔEp separation and I_a^p/I_c^p ratio, as well as the linear variation of I_a^pversus $\nu^{1/2}$ for both the electrodes, refer to a quasi-reversible redox system, corroborating other studies on DA detection on H- and O-terminated BDD films [28,87–89]. However, while D_EP generates cycles with sharp anodic peaks and low ΔEp separation, higher peak currents are detected by D_NaOH at each investigated scan rate. This finding can be rationalized by the superior surface roughness exhibited by D_NaOH, which can offer a greater number of active sites for electron transfer, as well as by the larger presence of surface sp^2 impurities of carbon, which probably facilitate the DA adsorption on the this electrode [89]. Another factor not to be disregarded is certainly the attraction exerted by the C—O moieties exhibited by the electrode. Although the electron transfer is commonly hampered on highly oxidized diamond surfaces, on the other hand the abundance of oxygenated functionalities of D_NaOH can enhance the electrostatic interactions with the resulting positively charged DA molecules at pH 7.4. A similar behavior was pointed out by Li et al. who demonstrated a high DA sensitivity for BDD electrodes surfaces characterized by a consistent abundance of oxygen-containing functionalities [9]. The selectivity versus DA was explored by SWV measurements in 10 mM PBS solution under the presence of the interferent agents, uric acid (UA) and ascorbic acid (AA), both at 1500 μM. Concentration dependence was studied up to 100 μM DA, being the latter a value that covers and even exceeds dopamine levels in neural tissues (typically a few μM units) (Fig. 7a, b). The SWV curves were processed by subtracting the baseline derived from the curve recorded in a 10 mM PBS reference solution. The response separately given by each single analyte on each electrode can be found in Fig. S1 while the stability of the analytical response was evaluated for the 0.1 mM DA concentration by performing five consecutive SWV measurements (Fig. S2). The reproducibility was tested by verifying the similar increase of the DA peak current as a function of the DA concentration for three different replicas of each typology of electrode. In Fig. 7c, d the linear fittings of

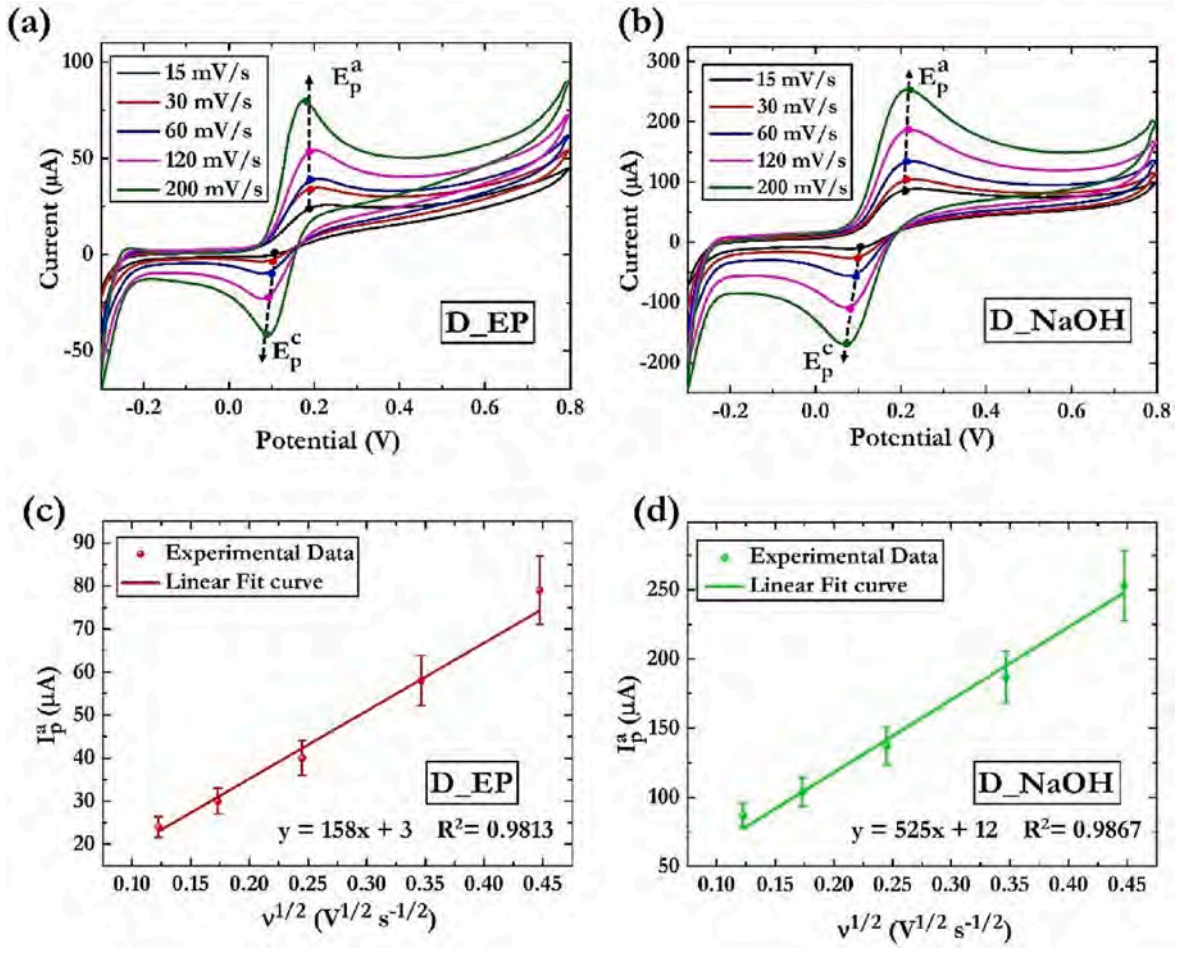

Fig. 6. Cyclic voltammograms of 1 mM dopamine in 10 mM PBS solution at pH 7.4 recorded at the scan rate of 15, 30, 60, 120 and 200 mV s^{-1} by (a) D_EP and (b) D_NaOH electrode. Linear fitting of I_a^p as a function of the square root of the scan rates ($\nu^{1/2}$) for (c) D_EP and (d) D_NaOH electrode.

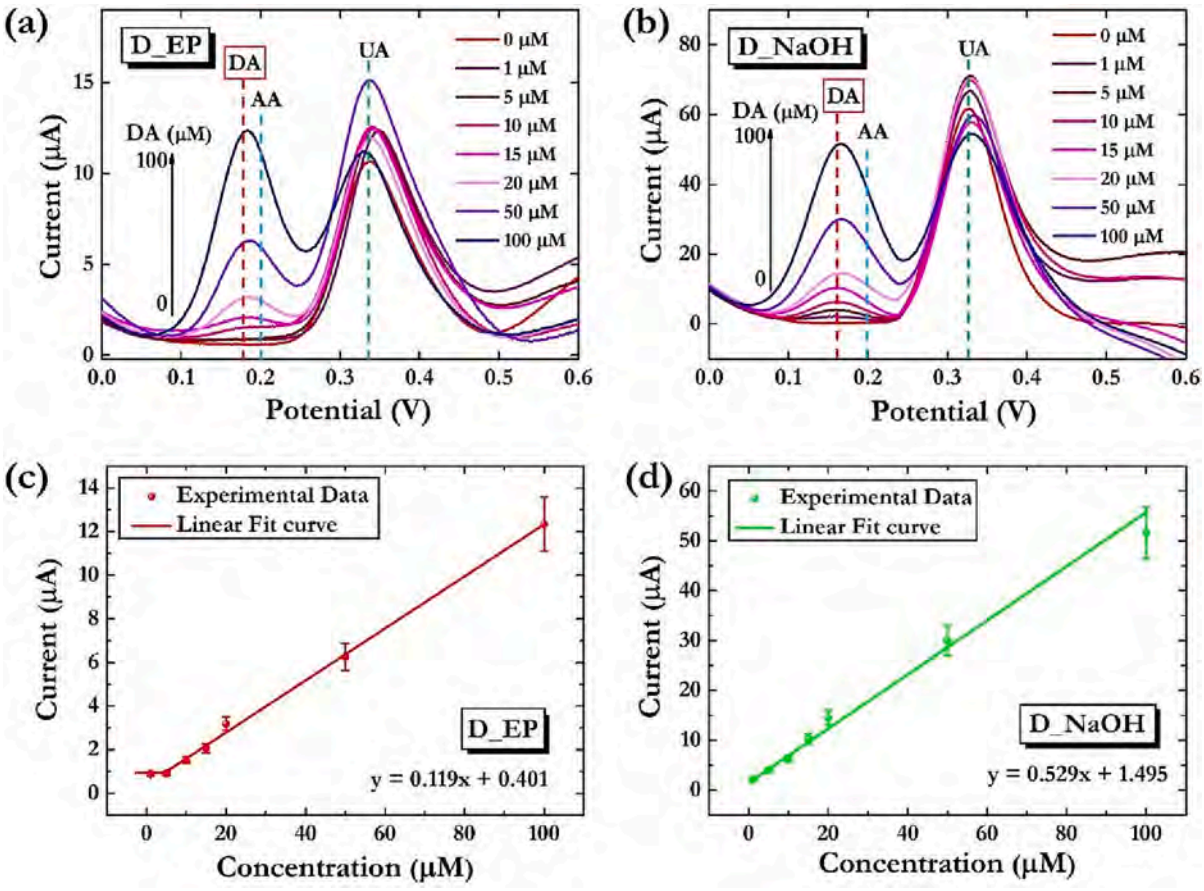

Fig. 7. SWV curves to detect DA in the concentration range (1 ÷ 100) μM in 10 mM PBS at pH 7.4 containing AA and UA both at 1500 μM AA recorded on (a) D_EP and (b) D_NaOH electrode; linear fitting of the peak current of SWV curve as a function of DA concentrations for (c) D_EP and (d) D_NaOH samples.

the peak currents versus DA concentrations are reported.

From Fig. 7a–b the SWV oxidation peaks of DA and UA are distinguishable on both D_EP and D_NaOH electrodes at about +0.17 and +0.35 V, respectively. The separation between these E_p^a values results on the order of 160 mV, in accordance with what has been observed in other studies [3–5,52,88,90]. Under the reported experimental conditions, the AA interferent appears instead to be undetectable on both the electrodes and remains so up to a concentration of 3000 μM (see Fig. S1). Observing the trend of the SWV peak current with the DA concentration (Fig. 7c, d), we note that D_EP shows a well-defined two-trends response, in which an initial noise regime, characterized by the indistinguishability of the signal intensity respect to the chemical and electronic noise, is followed by a linear response curve. This transition, which for D_EP electrode occurs at 5 μM, is totally absent for D_NaOH that shows a perfectly linear response in the same dynamic range. Moreover, the entity of the linear fit slope of this latter electrode suggests a higher sensing efficiency respect to the D_EP one.

The sensitivity of the electrodes can be estimated from the slope (m) of the regression equation. On the basis of IUPAC definition, the limit of detection (LOD) value holds 3.3 s/m where m is the slope of the calibration curve and s is the standard deviation of five blank replicates [91–93]. We obtain a LOD of 6.10 and 0.63 μM for D_EP and D_NaOH, respectively. The correlation coefficient (R^2) values are 0.9973 and 0.9825 for D_EP and D_NaOH electrodes, respectively. In Table 1 are reported the data for the linear dynamic range [94], linear regression equations, sensitivities, LOD and R^2 for DA detection in the presence of the interfering agents for both D_EP and D_NaOH electrode.

The sensitivities, LOD value and quite large linear detection range (1–100 μM) derived for D_NaOH electrode are in line with what found for other DA sensors [4,5,7–9,73,89,95]. Specifically, the peculiar properties of D_NaOH electrode allow for DA detection under AA and UA excess and with a LOD competitive with that of unmodified BDD [4,5,7–9,73]. To support the proposed detection mechanisms, EIS measurements were also conducted in PBS solution prior and after SWV measurements (Fig. S3). No appreciable differences can be evidenced before or after the DA detection in the presence of AA and AU interferent agents, confirming that the mechanism involved in the sensing activity cannot be related to physical-chemical absorption neither to intercalation nor coordination processes. All these outcomes clearly evidence the feasibility to exploit the D_NaOH electrode for assembling dopamine sensing devices.

Table 1
Linear dynamic range, linear regression equations, sensitivities, LOD and R^2 for the detection of DA in the presence of AA and AU interfering agents for D_EP and D_NaOH electrode.

Sample	Linear dynamic range	Linear regression equation	Sensitivity [A/M]	LOD [μM]	R^2
D_EP	17	0.119× + 0.401	0.119	6.10	0,9973
D_NaOH	167	0.529× + 1.495	0.529	0.63	0.9825

4. Conclusions

The present study aims to explore how the characteristics of CVD-grown boron free conductive diamond can be tailored to develop an electrode material for dopamine electrochemical detection. Three methods for Ti substrate polishing are tested: lapping, electropolishing, and electropolishing followed by 1 h soaking in 2 M NaOH solution kept

at 80 °C. The coupling of SEM, AFM, Raman spectroscopy XRD, XPS and I-V analyses demonstrated that the type of treatment is crucial to control the bulk as well as the surface features of the diamond films. D_LAP and D_EP are characterized by high phase purity, polycrystalline texture and surfaces almost completely constituted by C—C and C—H terminations. D_NaOH are formed by irregular deposits, constituted by diamond grains smaller than those of the other samples, low purity of the diamond phase and a 9 % relative concentration of the C—O moieties on the surfaces. The tuning of diamond properties is found to be critical for modulating the Ti-doped diamond electrodes' electrochemical performance, as evidenced by the estimation of k^0_{app} for the $Fe[(CN)_6]^{3-/4-}$ redox couple. On the other hand, SWV measurement demonstrated that the controlled introduction of C—O moieties on diamond surface enhances its selectivity versus DA detection in the presence of interferent agents such as the AA and UA. In fact, a 600 nM LOD and a sufficient linear range was achieved for D_NaOH electrode, evidencing its potential for DA sensing application.

In the light of the collected results, we can conclude that the overall properties of the boron free conductive CVD diamond can be effectively tailored solely by facile and low-cost substrate pretreatments. In this view, the absence of post-syntheses treatments, coupled with the biocompatibility and the tunability of the electrical and electrochemical properties of the produced samples, brings a new inspiration for developing diamond electrodes for a widespread range of technologies.

CRediT authorship contribution statement

Rocco Carcione: Conceptualization, Data curation, Formal analysis, Investigation, Methodology, Software, Writing – original draft. **Silvia Battistoni:** Conceptualization, Data curation, Investigation, Supervision, Validation, Visualization, Writing – review & editing. **Elena Palmieri:** Investigation, Methodology, Software, Writing – original draft. **Silvia Orlanducci:** Conceptualization, Data curation, Supervision, Validation, Visualization. **Emanuela Tamburri:** Conceptualization, Data curation, Supervision, Validation, Visualization, Writing – review & editing, Funding acquisition.

Declaration of competing interest

The authors declare that they have no known competing financial interests or personal relationships that could have appeared to influence the work reported in this paper.

Data availability

Data will be made available on request.

Acknowledgements

The authors are grateful to Professor Maria Letizia Terranova for her encouragement and suggestions, leading to the publication of this paper. The authors wish to acknowledge Fondazione Bruno Kessler (FBK, Trento, Italy) for assistance with AFM, XPS and XRD measurements. RC is grateful to FBK for financial support.

Appendix A. Supplementary data

Supplementary data to this article can be found online at https://doi.org/10.1016/j.surfcoat.2023.129662.

References

[1] J. Xu, Y. Yokota, R.A. Wong, Y. Kim, Y. Einaga, Unusual electrochemical properties of low-doped boron-doped diamond electrodes containing sp2 carbon, J. Am. Chem. Soc. 142 (2020) 2310–2316, https://doi.org/10.1021/JACS.9B11183/SUPPL_FILE/JA9B11183_SI_001.PDF.

[2] P.V. Nidheesh, G. Divyapriya, N. Oturan, C. Trellu, M.A. Oturan, Environmental applications of boron-doped diamond electrodes: 1. Applications in water and wastewater treatment, ChemElectroChem. 6 (2019) 2124–2142, https://doi.org/10.1002/CELC.201801876.

[3] S. Baluchová, A. Daňhel, H. Dejmková, V. Ostatná, M. Fojta, K. Schwarzová-Pecková, Recent progress in the applications of boron doped diamond electrodes in electroanalysis of organic compounds and biomolecules – a review, Anal. Chim. Acta 1077 (2019) 30–66, https://doi.org/10.1016/J.ACA.2019.05.041.

[4] S. Baluchová, M. Brycht, A. Taylor, V. Mortet, J. Krůšek, I. Dittert, S. Sedláková, L. Klimša, J. Kopeček, K. Schwarzová-Pecková, Enhancing electroanalytical performance of porous boron-doped diamond electrodes by increasing thickness for dopamine detection, Anal. Chim. Acta 1182 (2021), 338949, https://doi.org/10.1016/J.ACA.2021.338949.

[5] H. Li, K. Zhou, J. Cao, Q. Wei, C. Te Lin, S.E. Pei, L. Ma, N. Hu, Y. Guo, Z. Deng, Z. Yu, S. Zeng, W. Yang, L. Meng, A novel modification to boron-doped diamond electrode for enhanced, selective detection of dopamine in human serum, Carbon N. Y. 171 (2021) 16–28, https://doi.org/10.1016/J.CARBON.2020.08.019.

[6] D.F. Davidson, Elevated urinary dopamine in adults and children 42 (3) (2005) 200–207 (https://journals.sagepub.com/doi/pdf/10.1258/0004563053857851).

[7] H. Li, J. Cao, Q. Wei, L. Ma, K. Zhou, Z. Yu, S. Zeng, R. Zhu, W. Yang, C. Te Lin, L. Meng, Antifouling nanoporous diamond membrane for enhanced detection of dopamine in human serum, J. Mater. Sci. 56 (2021) 746–761, https://doi.org/10.1007/S10853-020-05344-5.

[8] H. Li, Y. Guo, S. Zeng, Q. Wei, P.E. Sharel, R. Zhu, J. Cao, L. Ma, K.C. Zhou, L. Meng, High-sensitivity, selective determination of dopamine using bimetallic nanoparticles modified boron-doped diamond electrode with anodic polarization treatment, J. Mater. Sci. 56 (2021) 4700–4715, https://doi.org/10.1007/S10853-020-05577-4/FIGURES/8.

[9] Y. Li, H. Li, M. Li, C. Li, D. Sun, B. Yang, Porous boron-doped diamond electrode for detection of dopamine and pyridoxine in human serum, Electrochim. Acta 258 (2017) 744–753, https://doi.org/10.1016/J.ELECTACTA.2017.11.121.

[10] G. Polino, A. Scaramella, V. Manca, E. Palmieri, E. Tamburri, S. Orlanducci, F. Brunetti, Nanodiamond-based separators for supercapacitors realized on paper substrates, Energy Technol. 8 (2020) (https://onlinelibrary.wiley.com/doi/10.1002/ente.201901233).

[11] X.R. Lu, M.H. Ding, C. Zhang, W.Z. Tang, Investigation on microstructure evolution and failure mechanism of boron doped diamond coated titanium electrode during accelerated life test, Thin Solid Films 660 (2018) 306–313, https://doi.org/10.1016/J.TSF.2018.06.039.

[12] C. Zhang, X. Lu, Y. Lu, M. Ding, W. Tang, Titanium-boron doped diamond composite: a new anode material, Diam. Relat. Mater. 98 (2019), 107490, https://doi.org/10.1016/J.DIAMOND.2019.107490.

[13] K. Fabisiak, M. Kowalska, M. Szybowicz, K. Paprocki, P. Popielarski, A. Wrzyszczyński, L. Mosińska, G.K. Zhusupkalieva, The undoped CVD diamond electrode: the effect of surface pretreatment on its electrochemical properties, Adv. Eng. Mater. 15 (2013) 935–940, https://doi.org/10.1002/ADEM.201200351.

[14] S. Ferro, M. Dal Colle, A. De Battisti, Chemical surface characterization of electrochemically and thermally oxidized boron-doped diamond film electrodes, Carbon N. Y. 43 (2005) 1191–1203, https://doi.org/10.1016/J.CARBON.2004.12.012.

[15] S. Meijs, M. Alcaide, C. Sørensen, M. McDonald, S. Sørensen, K. Rechendorff, A. Gerhardt, M. Nesladek, N.J.M. Rijkhoff, C.P. Pennisi, Biofouling resistance of boron-doped diamond neural stimulation electrodes is superior to titanium nitride electrodes in vivo, J. Neural Eng. (2016), https://doi.org/10.1088/1741-2560/13/5/056011.

[16] J. Ryl, L. Burczyk, R. Bogdanowicz, M. Sobaszek, K. Darowicki, Study on surface termination of boron-doped diamond electrodes under anodic polarization in H2SO4 by means of dynamic impedance technique, Carbon N. Y. 96 (2016) 1093–1105, https://doi.org/10.1016/J.CARBON.2015.10.064.

[17] L. Grausova, A. Kromka, Z. Burdikova, A. Eckhardt, B. Rezek, J. Vacik, K. Haenen, V. Lisa, L. Bacakova, Enhanced growth and osteogenic differentiation of human osteoblast-like cells on boron-doped nanocrystalline diamond thin films, PLoS One 6 (2011), e20943, https://doi.org/10.1371/journal.pone.0020943.

[18] L.J. Simcox, R.P.A. Pereira, E.M.H. Wellington, J.V. Macpherson, Boron doped diamond as a low biofouling material in aquatic environments: assessment of *Pseudomonas aeruginosa* biofilm formation, ACS Appl. Mater. Interfaces (2019), https://doi.org/10.1021/acsami.9b07245.

[19] Y. Dai, D.A. Proshlyakov, G.M. Swain, Effects of film morphology and surface chemistry on the direct electrochemistry of cytochrome c at boron-doped diamond electrodes, Electrochim. Acta 197 (2016) 129–138, https://doi.org/10.1016/J.ELECTACTA.2016.02.032.

[20] O. Romanyuk, I. Bartoš, I. Gordeev, A. Artemenko, M. Varga, T. Ižák, M. Marton, P. Jiříček, A. Kromka, Electron affinity of undoped and boron-doped polycrystalline diamond films, Diam. Relat. Mater. 87 (2018) 208–214, https://doi.org/10.1016/J.DIAMOND.2018.06.005.

[21] C.W. Song, D.S. Cho, J.M. Lee, P.K. Song, Effect of Boron Doping on Diamond Film and Electrochemical Properties of BDD According to Thickness and Morphology, (n.d.). doi:https://doi.org/10.3390/coatings10040331.

[22] S. Li, J. Wang, M. Hu, M. Li, X. Liu, T. Su, K. Yu, F. Han, The first principle study and experimental of boron synergistic sulfur doping in diamond, Mater. Today Commun. 24 (2020), 101021, https://doi.org/10.1016/J.MTCOMM.2020.101021.

[23] J. Weng, J. Xue, J. Wang, J.S. Ye, H. Cui, F.S. Sheu, Q. Zhang, Gold-cluster sensors formed electrochemically at boron-doped-diamond electrodes: detection of dopamine in the presence of ascorbic acid and thiols, Adv. Funct. Mater. 15 (2005) 639–647, https://doi.org/10.1002/ADFM.200400049.

[24] J. Svítková, T. Ignat, Ľ. Švorc, J. Labuda, J. Barek, Chemical Modification of Boron-Doped Diamond Electrodes for Applications to Biosensors and Biosensing 46, 2016, pp. 248–256, https://doi.org/10.1080/10408347.2015.1082125.
[25] E. Popa, H. Notsu, T. Miwa, D.A. Tryk, A. Fujishima, Selective electrochemical detection of dopamine in the presence of ascorbic acid at anodized diamond thin film electrodes, Electrochem. Solid-State Lett. 2 (1999) 49–51, https://doi.org/10.1149/1.1390730/XML.
[26] L. Jiang, G.W. Nelson, J. Abda, J.S. Foord, Novel modifications to carbon-based electrodes to improve the electrochemical detection of dopamine, ACS Appl. Mater. Interfaces 8 (2016) 28338–28348, https://doi.org/10.1021/ACSAMI.6B03879/SUPPL_FILE/AM6B03879_SI_001.PDF.
[27] F. Shang, Y. Liu, S. Hrapovic, J.D. Glennon, J.H.T. Luong, Selective detection of dopamine using a combined permselective film of electropolymerized (poly-tyramine and poly-pyrrole-1-propionic acid) on a boron-doped diamond electrode, Analyst. 134 (2009) 519–527, https://doi.org/10.1039/B814317J.
[28] K. Yao, X. Tan, B. Dai, J. Bai, Q. Sun, W. Cao, J. Zhao, L. Yang, J. Han, J. Zhu, Au nanospheres modified boron-doped diamond microelectrode grown via hydrogen plasma etching solid doping source for dopamine detection, J. Mater. Sci. Technol. 49 (2020) 42–46, https://doi.org/10.1016/J.JMST.2020.02.003.
[29] M. Werner, R. Locher, W. Kohly, D.S. Holmes, S. Klose, H.J. Fecht, The diamond Irvin curve, Diam. Relat. Mater. 6 (1997) 308–313, https://doi.org/10.1016/S0925-9635(96)00683-8.
[30] K.B. Holt, A.J. Bard, Y. Show, G.M. Swain, Scanning Electrochemical Microscopy and Conductive Probe Atomic Force Microscopy Studies of Hydrogen-Terminated Boron-Doped Diamond Electrodes with Different Doping Levels, 2004, https://doi.org/10.1021/jp048222x.
[31] A.N. Ndao, F. Zenia, A. Deneuville, M. Bernard, C. Lévy-Clément, Effect of boron concentration on the electrochemical reduction of nitrates on polycrystalline diamond electrodes, Diam. Relat. Mater. 9 (2000) 1175–1180, https://doi.org/10.1016/S0925-9635(99)00328-3.
[32] N.G. Ferreira, L.L.G. Silva, E.J. Corat, V.J. Trava-Airoldi, Kinetics study of diamond electrodes at different levels of boron doping as quasi-reversible systems, Diam. Relat. Mater. 11 (2002) 1523–1531, https://doi.org/10.1016/S0925-9635(02)00060-2.
[33] A.E. Fischer, Y. Show, G.M. Swain, Electrochemical performance of diamond thin-film electrodes from different commercial sources, Anal. Chem. 76 (2004) 2553–2560, https://doi.org/10.1021/AC035214O/SUPPL_FILE/AC035214OSI20040218_051807.PDF.
[34] N. Hadrup, M. Frederiksen, A.K. Sharma, Toxicity of boric acid, borax and other boron containing compounds: a review, Regul. Toxicol. Pharmacol. 121 (2021), 104873, https://doi.org/10.1016/J.YRTPH.2021.104873.
[35] R. Carcione, S. Politi, E. Iacob, C. Potrich, L. Lunelli, L.E. Vanzetti, R. Bartali, V. Micheli, G. Pepponi, M.L. Terranova, E. Tamburri, Exploring a new approach for regenerative medicine: Ti-doped polycrystalline diamond layers as bioactive platforms for osteoblast-like cells growth, Appl. Surf. Sci. (2021), https://doi.org/10.1016/j.apsusc.2020.148334.
[36] E. Tamburri, R. Carcione, F. Vitale, A. Valguarnera, S. Macis, M. Lucci, M. L. Terranova, Exploiting the properties of Ti-doped CVD-grown diamonds for the assembling of electrodes, Adv. Mater. Interfaces 4 (2017) 1700222, https://doi.org/10.1002/admi.201700222.
[37] S. Mandal, Nucleation of diamond films on heterogeneous substrates: a review, RSC Adv. 11 (2021) 10159–10182, https://doi.org/10.1039/D1RA00397F.
[38] M. Panizza, G. Cerisola, Application of diamond electrodes to electrochemical processes, Electrochim. Acta 51 (2005) 191–199, https://doi.org/10.1016/J.ELECTACTA.2005.04.023.
[39] M. Terranova, S. Piccirillo, … V.S.-D. and related, undefined 2001, Electrochemical Behaviour of Electrodes Assembled with Ti-containing Diamond Films, Elsevier. (n. d.). https://www.sciencedirect.com/science/article/pii/S0925963500004350 (accessed April 5, 2022).
[40] M.L. Terranova, V. Sessa, S. Piccirillo, M. Rossi, G. Micocci, A. Serra, A. Tepore, Unusual electrical behavior of Nd-doped diamond films, Appl. Phys. Lett. 75 (1999) 379–381, https://doi.org/10.1063/1.124381.
[41] R. Carcione, E. Tamburri, R. Bartali, G. Speranza, V. Micheli, G. Pepponi, P. Bellutti, M.L. Terranova, On the route to produce conductive Ni-related color centers in CVD-grown diamond, Multifunct. Mater. 2 (2019), https://doi.org/10.1088/2399-7532/ab2c35.
[42] A. Rifai, N. Tran, P. Reineck, A. Elbourne, E. Mayes, A. Sarker, C. Dekiwadia, E. P. Ivanova, R.J. Crawford, T. Ohshima, B.C. Gibson, A.D. Greentree, E. Pirogova, K. Fox, Engineering the interface: nanodiamond coating on 3D-printed titanium promotes mammalian cell growth and inhibits *Staphylococcus aureus* colonization, ACS Appl. Mater. Interfaces (2019), https://doi.org/10.1021/acsami.9b07064.
[43] K. Fox, N. Mani, A. Rifai, P. Reineck, A. Jones, P.A. Tran, A. Ramezannejad, M. Brandt, B.C. Gibson, A.D. Greentree, N. Tran, 3D-printed diamond-titanium composite: a hybrid material for implant engineering, ACS Appl. Bio Mater. (2020), https://doi.org/10.1021/acsabm.9b00801.
[44] M.A. Booth, L. Pope, P.C. Sherrell, A. Stacey, P.A. Tran, K.E. Fox, Polycrystalline diamond coating on 3D printed titanium scaffolds: surface characterisation and foreign body response, Mater. Sci. Eng. C. 130 (2021), 112467, https://doi.org/10.1016/j.msec.2021.112467.
[45] D. Sur, P. Tirado, J. Alcantar, O. Auciello, G.B. Basim, Integration of ultrananocrystalline diamond (UNCD)-coatings on chemical-mechanical surface Nano-structured (CMNS) titanium-based dental implants, MRS Adv. (2020), https://doi.org/10.1557/adv.2020.329.
[46] S. Battistoni, R. Carcione, E. Tamburri, V. Erokhin, M.L. Terranova, S. Iannotta, A Ti-doped chemical vapor deposition diamond device as artificial synapse for neuromorphic applications, Adv. Mater. Technol. (2023) 2201555, https://doi.org/10.1002/admt.202201555.
[47] S. Shen, W. Shen, S. Liu, H. Li, Y. Chen, H. Qi, First-principles calculations of co-doping impurities in diamond, Mater. Today Commun. 23 (2020), 100847, https://doi.org/10.1016/J.MTCOMM.2019.100847.
[48] J.P. Goss, P.R. Briddon, R. Jones, S. Sque, Donor and acceptor states in diamond, Diam. Relat. Mater. 13 (2004) 684–690, https://doi.org/10.1016/j.diamond.2003.08.028.
[49] M. Hupert, A. Muck, J. Wang, J. Stotter, Z. Cvackova, S. Haymond, Y. Show, G. M. Swain, Conductive diamond thin-films in electrochemistry, Diam. Relat. Mater. 12 (2003) 1940–1949, https://doi.org/10.1016/S0925-9635(03)00260-7.
[50] G. Dutta, S. Siddiqui, H. Zeng, J.A. Carlisle, P.U. Arumugam, The effect of electrode size and surface heterogeneity on electrochemical properties of ultrananocrystalline diamond microelectrode, J. Electroanal. Chem. 756 (2015) 61–68, https://doi.org/10.1016/J.JELECHEM.2015.08.016.
[51] R.C. Alkire, P.N. Bartlett, J. Lipkowski (Eds.), Electrochemistry of Carbon Electrodes, 2015, https://doi.org/10.1002/9783527697489.
[52] E. Popa, Y. Kubota, D.A. Tryk, A. Fujishima, Selective voltammetric and amperometric detection of uric acid with oxidized diamond film electrodes, Anal. Chem. 72 (2000) 1724–1727, https://doi.org/10.1021/ac990862m.
[53] G.R. Salazar-Banda, L.S. Andrade, P.A.P. Nascente, P.S. Pizani, R.C. Rocha-Filho, L. A. Avaca, On the changing electrochemical behaviour of boron-doped diamond surfaces with time after cathodic pre-treatments, Electrochim. Acta 51 (2006) 4612–4619, https://doi.org/10.1016/J.ELECTACTA.2005.12.039.
[54] J.O. Thostenson, E. Ngaboyamahina, K.L. Sellgren, B.T. Hawkins, J.R. Piascik, E.J. D. Klem, C.B. Parker, M.A. Deshusses, B.R. Stoner, J.T. Glass, Enhanced H2O2 production at reductive potentials from oxidized boron-doped ultrananocrystalline diamond electrodes, ACS Appl. Mater. Interfaces 9 (2017) 16610–16619, https://doi.org/10.1021/ACSAMI.7B01614/SUPPL_FILE/AM7B01614_SI_001.PDF.
[55] N. Tokuda, H. Umezawa, S.G. Ri, K. Yamabe, H. Okushi, S. Yamasaki, Roughening of atomically flat diamond (111) surfaces by a hot HNO3/H2SO4 solution, Diam. Relat. Mater. 17 (2008) 486–488, https://doi.org/10.1016/J.DIAMOND.2008.01.042.
[56] X. Wang, A.R. Ruslinda, Y. Ishiyama, Y. Ishii, H. Kawarada, Higher coverage of carboxylic acid groups on oxidized single crystal diamond (001), Diam. Relat. Mater. 20 (2011) 1319–1324, https://doi.org/10.1016/J.DIAMOND.2011.08.011.
[57] F. Klauser, S. Ghodbane, R. Boukherroub, S. Szunerits, D. Steinmüller-Nethl, E. Bertel, N. Memmel, Comparison of different oxidation techniques on single-crystal and nanocrystalline diamond surfaces, Diam. Relat. Mater. 19 (2010) 474–478, https://doi.org/10.1016/J.DIAMOND.2009.11.013.
[58] R. Boukherroub, X. Wallart, S. Szunerits, B. Marcus, P. Bouvier, M. Mermoux, Photochemical oxidation of hydrogenated boron-doped diamond surfaces, Electrochem. Commun. 7 (2005) 937–940, https://doi.org/10.1016/J.ELECOM.2005.05.010.
[59] M. Jiang, H. Yu, X. Li, S. Lu, X. Hu, Thermal oxidation induced high electrochemical activity of boron-doped nanocrystalline diamond electrodes, Electrochim. Acta 258 (2017) 61–70, https://doi.org/10.1016/J.ELECTACTA.2017.10.008.
[60] C. Li, X. Zhang, E.F. Oliveira, A.B. Puthirath, M.R. Neupane, J.D. Weil, A. G. Birdwell, T.G. Ivanov, S. Kong, T. Gray, H. Kannan, A. Biswas, R. Vajtai, D. S. Galvao, P.M. Ajayan, Systematic comparison of various oxidation treatments on diamond surface, Carbon N. Y. 182 (2021) 725–734, https://doi.org/10.1016/J.CARBON.2021.06.050.
[61] A. Dychalska, M. Trzcinski, K. Fabisiak, K. Paprocki, W. Koczorowski, S. Łoś, M. Szybowicz, The effect of UV and thermally induced oxidation on the surface and structural properties of CVD diamond layers with different grain sizes, Diam. Relat. Mater. 121 (2022), 108739, https://doi.org/10.1016/J.DIAMOND.2021.108739.
[62] J. Raymakers, K. Haenen, W. Maes, Diamond surface functionalization: from gemstone to photoelectrochemical applications, J. Mater. Chem. C 7 (2019) 10134–10165, https://doi.org/10.1039/C9TC03381E.
[63] C. Pietzka, A. Denisenko, A. Romanyuk, P.J. Schäfer, L.A. Kibler, J. Scharpf, E. Kohn, Electronic surface barrier properties of boron-doped diamond oxidized by plasma treatment, Diam. Relat. Mater. 19 (2010) 213–216, https://doi.org/10.1016/J.DIAMOND.2009.08.014.
[64] K. Ueda, K. Kawamoto, H. Asano, High-temperature and high-voltage characteristics of Cu/diamond Schottky diodes, Diam. Relat. Mater. 57 (2015) 28–31, https://doi.org/10.1016/J.DIAMOND.2015.03.006.
[65] A. Polyakov, N. Smirnov, S. Tarelkin, A. Govorkov, V. Bormashov, M. Kuznetsov, D. Teteruk, S. Buga, N. Kornilov, I.H. Lee, Electrical properties of diamond platinum vertical Schottky barrier diodes, Mater. Today Proc. 3 (2016) S159–S164, https://doi.org/10.1016/J.MATPR.2016.02.027.
[66] J. Navas, D. Araujo, J.C. Piñero, A. Sánchez-Coronilla, E. Blanco, P. Villar, R. Alcántara, J. Montserrat, M. Florentin, D. Eon, J. Pernot, Oxygen termination of homoepitaxial diamond surface by ozone and chemical methods: an experimental and theoretical perspective, Appl. Surf. Sci. 433 (2018) 408–418, https://doi.org/10.1016/J.APSUSC.2017.10.065.
[67] M. Wang, N. Simon, C. Decorse-Pascanut, M. Bouttemy, A. Etcheberry, M. Li, R. Boukherroub, S. Szunerits, Comparison of the chemical composition of boron-doped diamond surfaces upon different oxidation processes, Electrochim. Acta 54 (2009) 5818–5824, https://doi.org/10.1016/J.ELECTACTA.2009.05.037.
[68] J. Xu, K. Lu, D. Fan, Y. Wang, S. Xu, M. Kubo, Different etching mechanisms of diamond by oxygen and hydrogen plasma: a reactive molecular dynamics study, J. Phys. Chem. C 125 (2021) 16711–16718, https://doi.org/10.1021/ACS.JPCC.1C03919/SUPPL_FILE/JP1C03919_SI_001.PDF.
[69] N. Tokuda, D. Takeuchi, S.G. Ri, H. Umezawa, K. Yamabe, H. Okushi, S. Yamasaki, Flattening of oxidized diamond (111) surfaces with H2SO4/H2O2 solutions, Diam.

Relat. Mater. 18 (2009) 213–215, https://doi.org/10.1016/J.DIAMOND.2008.10.010.
[70] S.J. Cobb, F.H.J. Laidlaw, G. West, G. Wood, M.E. Newton, R. Beanland, J. V. Macpherson, Assessment of acid and thermal oxidation treatments for removing sp2 bonded carbon from the surface of boron doped diamond, Carbon N. Y. 167 (2020) 1–10, https://doi.org/10.1016/J.CARBON.2020.04.095.
[71] Y. Hang Liu, J. Liang Zhang, F. Liang Wu, M. Qi, L. Fu Hei, F. Xiu Lv, The Raman spectroscopy and XPS investigation of CVD diamond after fast-neutron irradiation, Mater. Today Commun. 22 (2020), 100699, https://doi.org/10.1016/J.MTCOMM.2019.100699.
[72] C.E. Nebel, D. Shin, B. Rezek, N. Tokuda, H. Uetsuka, H. Watanabe, Diamond and biology, J. R. Soc. Interface 4 (2007) 439–461, https://doi.org/10.1098/RSIF.2006.0196.
[73] Z. Yang, M. Li, H. Li, H. Li, C. Li, B. Yang, Polycrystalline boron-doped diamond-based electrochemical biosensor for simultaneous detection of dopamine and melatonin, Anal. Chim. Acta 1135 (2020) 73–82, https://doi.org/10.1016/J.ACA.2020.08.042.
[74] S. Prawer, R.J. Nemanich, Raman spectroscopy of diamond and doped diamond, Philos. Trans. R. Soc. A Math. Phys. Eng. Sci. (2004), https://doi.org/10.1098/rsta.2004.1451.
[75] A.C. Ferrari, J. Robertson, Resonant Raman spectroscopy of disordered, amorphous, and diamondlike carbon, Phys. Rev. B - Condens. Matter Mater. Phys. (2001), https://doi.org/10.1103/PhysRevB.64.075414.
[76] S.M. Leeds, T.J. Davis, P.W. May, C.D.O. Pickard, M.N.R. Ashfold, Use of different excitation wavelengths for the analysis of CVD diamond by laser Raman spectroscopy, Diam. Relat. Mater. (1998), https://doi.org/10.1016/s0925-9635(97)00261-6.
[77] W. Fortunato, A.J. Chiquito, J.C. Galzerani, J.R. Moro, Crystalline quality and phase purity of CVD diamond films studied by Raman spectroscopy, J. Mater. Sci. (2007), https://doi.org/10.1007/s10853-007-1575-0.
[78] L.M. Da Silva, D.A.D.L. Almeida, A.B. Couto, N.G. Ferreira, Morphological, structural and electrochemical characterizations of PAni/BDND/CF ternary composite, Diam. Relat. Mater. (2016), https://doi.org/10.1016/j.diamond.2016.03.008.
[79] S. Politi, S. Battistoni, R. Carcione, L. Montaina, S. Macis, S. Lupi, E. Tamburri, PANI-modified Ti-doped CVD diamond as promising conductive platform to mimic bioelectricity functions, Adv. Mater. Interfaces 8 (2021) 2101401 (https://onlinelibrary.wiley.com/doi/10.1002/admi.202101401).
[80] M. Ali, M. Ürgen, Surface morphology, growth rate and quality of diamond films synthesized in hot filament CVD system under various methane concentrations, Appl. Surf. Sci. 257 (2011) 8420–8426, https://doi.org/10.1016/J.APSUSC.2011.04.097.
[81] S. Orlanducci, A. Fiori, V. Sessa, E. Tamburri, F. Toschi, M.L. Terranova, Nanocrystalline diamond films grown in nitrogen rich atmosphere: structural and field emission properties, J. Nanosci. Nanotechnol. 8 (2008) 3228–3234, https://doi.org/10.1166/JNN.2008.154.
[82] V. Vorlíček, J. Rosa, M. Vaněček, M. Nesládek, L.M. Stals, Quantitative study of Raman scattering and defect optical absorption in CVD diamond films, Diam. Relat. Mater. 6 (1997) 704–707, https://doi.org/10.1016/S0925-9635(96)00630-9.
[83] C. Wild, N. Herres, P. Koidl, Texture formation in polycrystalline diamond films, J. Appl. Phys. 68 (1998) 973, https://doi.org/10.1063/1.346663.
[84] S. Yugo, T. Kimura, T. Kanai, Nucleation mechanisms of diamond in plasma chemical vapor deposition, Diam. Relat. Mater. 2 (1993) 328–332, https://doi.org/10.1016/0925-9635(93)90076-E.
[85] X. Liu, P. Lu, H. Wang, Y. Ren, X. Tan, S. Sun, H. Jia, Morphology and structure of Ti-doped diamond films prepared by microwave plasma chemical vapor deposition, Appl. Surf. Sci. 442 (2018) 529–536, https://doi.org/10.1016/j.apsusc.2018.02.180.
[86] G. Alba, D. Eon, M.P. Villar, R. Alcántara, G. Chicot, J. Cañas, J. Letellier, J. Pernot, D. Araujo, H-terminated diamond surface band bending characterization by angle-resolved XPS, Surfaces. (2020), https://doi.org/10.3390/surfaces3010007.
[87] B. Fan, C.A. Rusinek, C.H. Thompson, M. Setien, Y. Guo, R. Rechenberg, Y. Gong, A.J. Weber, M.F. Becker, E. Purcell, W. Li, Flexible, diamond-based microelectrodes fabricated using the diamond growth side for neural sensing, Microsyst. Nanoeng. 61 (6) (2020) 1–12, https://doi.org/10.1038/s41378-020-0155-1.
[88] S. Baluchová, A. Taylor, V. Mortet, S. Sedláková, L. Klimša, J. Kopeček, O. Hák, K. Schwarzová-Pecková, Porous boron doped diamond for dopamine sensing: effect of boron doping level on morphology and electrochemical performance, Electrochim. Acta 327 (2019), 135025, https://doi.org/10.1016/J.ELECTACTA.2019.135025.
[89] M. Brycht, S. Baluchová, A. Taylor, V. Mortet, S. Sedláková, L. Klimša, J. Kopeček, K. Schwarzová-Pecková, Comparison of electrochemical performance of various boron-doped diamond electrodes: dopamine sensing in biomimicking media used for cell cultivation, Bioelectrochemistry. 137 (2021), 107646, https://doi.org/10.1016/J.BIOELECHEM.2020.107646.
[90] R. Kiran, E. Scorsone, P. Mailley, P. Bergonzo, Quasi-Real Time Quantification of Uric Acid in Urine Using Boron Doped Diamond Microelectrode with in Situ Cleaning, 2012, https://doi.org/10.1021/ac301177z.
[91] E. Ergün, Ş. Kart, D.K. Zeybek, B. Zeybek, Simultaneous electrochemical determination of ascorbic acid and uric acid using poly(glyoxal-bis(2-hydroxyanil)) modified glassy carbon electrode, Sensors Actuators B Chem. 224 (2016) 55–64, https://doi.org/10.1016/J.SNB.2015.10.032.
[92] C.J. Valentine, K. Takagishi, S. Umezu, R. Daly, M. De Volder, Paper-based electrochemical sensors using paper as a scaffold to create porous carbon nanotube electrodes, ACS Appl. Mater. Interfaces 12 (2020) 30680–30685, https://doi.org/10.1021/ACSAMI.0C04896/ASSET/IMAGES/LARGE/AM0C04896_0005.JPEG.
[93] A.B. Shehata, G.G. Mohamed, M.A. Gab-Allah, Simple spectrophotometric method for determination of iron in crude oil, Pet. Chem. 57 (2018) 1007–1011, 2017 5712, https://doi.org/10.1134/S096554411712012X.
[94] V. Gold (Ed.), The IUPAC Compendium of Chemical Terminology, International Union of Pure and Applied Chemistry (IUPAC), Research Triangle Park, NC, 2019, https://doi.org/10.1351/goldbook.
[95] K. Tyszczuk-Rotko, I. Jaworska, K. Jędruchniewicz, Application of unmodified boron-doped diamond electrode for determination of dopamine and paracetamol, Microchem. J. 146 (2019) 664–672, https://doi.org/10.1016/J.MICROC.2019.01.064.